# Report on the outcomes of a Short-Term Scientific Mission

**Action number: IG16215**

**Grantee name: Ahmad Abu Baker,** Faculty of Archaeology and Anthropology, Yarmouk University, Irbid, Jordan

**Details of the STSM**

**Title:** The use of MiCorr application to diagnose the corrosion of archaeological brass artefacts from Jordan

**Start and end date:** 01/06/2023 to 09/06/2023
**Location:** Haute Ecole Arc Conservation-restauration, Neuchâtel, Switzerland
**Scientific support:** Christian Degrigny (HE-Arc CR)
**Technical support:** Catherine Cséfalvay (Haute Ecole Ingénierie Arc)

**General programme:** The programme included two parts, the first was a training on *Discovery Mat* application and *Pleco* instrument. The Discovery Mat application was used to determine the composition of a copper alloy metal. The Pleco instrument was used to identify corrosion products formed on a tarnished silver coupon, and then to electrolytically reduce them in order to clean the silver surface.

The second part was devoted to using the *MiCorr* application to identify the family of metals studied, and then to create stratigraphic representations of the corrosion structures of two brass objects from Jordan in order to diagnose them.

**Description of the work carried out during the STSM**

**1) 1st of June:**

**- Basic training on Discovery Mat application for the analysis of metal and alloy compositions**

The process involved measuring the potential of the metal studied in three different solutions (Evian water, 1% wt./vol. potassium nitrate ($KNO_3$), and 1% wt./vol. sodium sesquicarbonate dihydrate ($Na_2CO_3.NaHCO_3.2H_2O$) using a Yoctopuce voltmeter connected to the laptop with the Discovery Mat application installed on it. The setup for the experiment included the metal, a silver/silver chloride (Ag/AgCl) reference electrode in a junction tube and a drop of the solution (20µL) between the metal surface and the frit of the junction of the reference electrode (Fig. 1). Before measuring the potential of the metal in each electrolyte, it was polished with SiC paper grade 4000 (Struers), rinsed with deionised water and dried. For each electrolyte, at least 3 potential scans were carried out, 2 for 5 minutes (300 measurement points) and 1 for 15 minutes (900 measurement points). It was important to check that the first two 5-minute plots were reproducible (i.e. that they overlapped or that their values were close and the plots parallel), and that the third 15-minute plot fell between the two. In some cases, a fourth plot was necessary because the third plot did not lie between the first two.

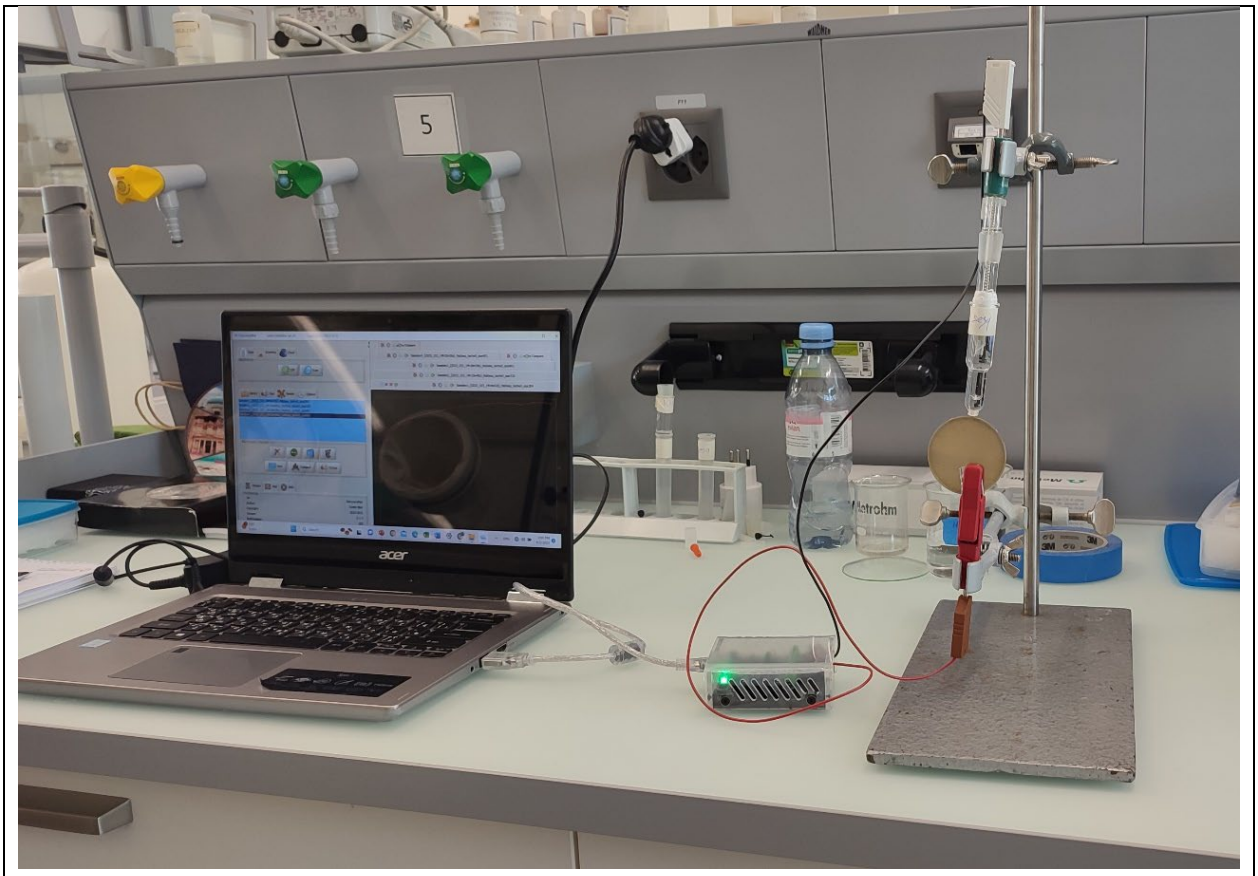


Fig. 1: Measurement of the metal potential in one of the electrolytes using the Discovery Mat application.

After completing the scans, those of 15 minutes representative of the behaviour of the metal in each of the 3 electrolytes were selected in the *sample* workspace of the application (Fig. 2) and transferred to the *Test* workspace. This was done by clicking on the (ToTest) button and the window shown in Fig. 3 appeared. Additional information associated to both 5 and 15 minutes plots was provided: reproducibility of the plots for each solution, presence or not of fluctuations of potentials and presence or not of a stain left by the solution on the metal surface. The window also showed the appearance of the three plots with their respective colours.

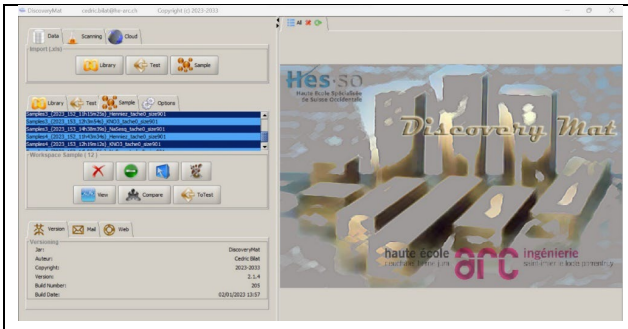


Fig. 2: Selecting the results in the *sample* workspace.

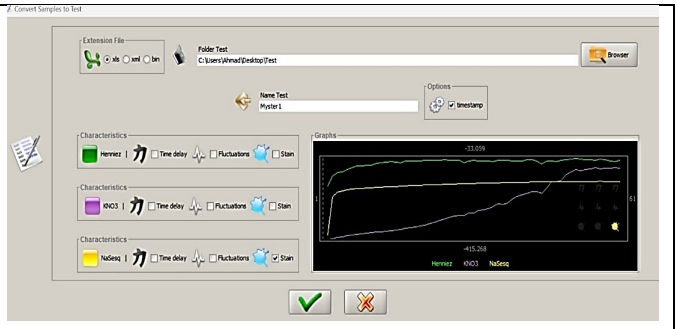


Fig. 3: Compilation of the three plots of the metal under investigation.

By clicking on the (√) button, the window shown in Fig. 4 appeared with the name of the Test material (Myster1) in the Test workspace and its plots in the three solutions considered on the right-hand side. This operation smoothed out the initial plots by reducing the measurements to only 60 points. The next step was to compare the test material to the 124 materials of Discovery Mat database. These materials of known composition (analysed with X-ray fluorescence) have been studied electrochemically using the same protocol. This was done by clicking on top menu on *Data*, and *Library* buttons, uploading the database from the operator's files (Fig. 5) and selecting all library results using the blue button (Select all items button) (Fig. 6).

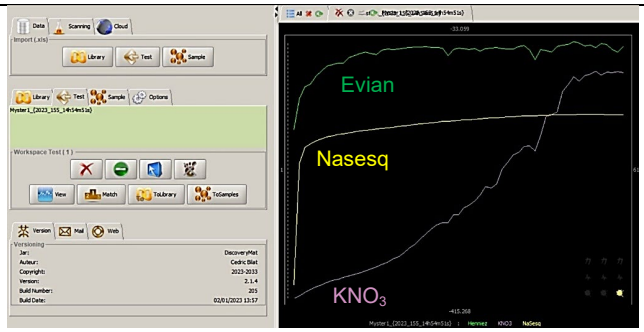


Fig. 4: Visualisation of the three plots of the metal under investigation and their characteristics in bottom right window.

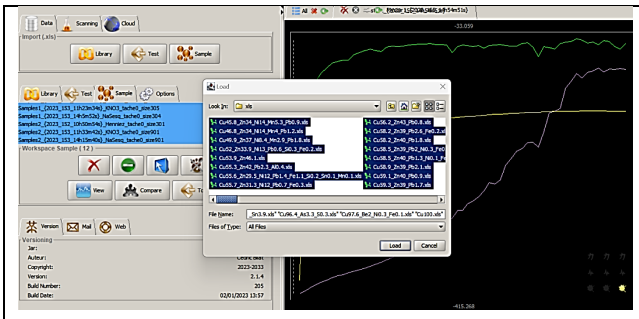

Fig. 5: Uploading the database under Library workspace.

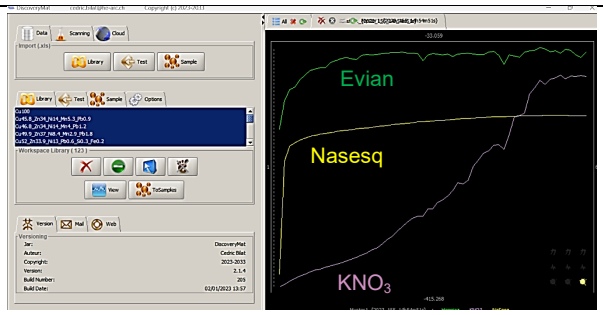


Fig. 6: Selecting all materials in the database for the comparison.

The plots of the test material were then compared to those of the materials in the database by returning to the Test workspace. After checking that the Myster1 is over-lit, the *Match* button was clicked. The application provided then two types of information: by clicking on the *Proposals* button in the right part of the screen, a list of proposed compositions was obtained. Each of them gives the distance between the plots of the material in the database and those of the metal under investigation (Fig. 7). The proposal 1 in the list is the most plausible, the last is the least. It is important to look at the first ten proposals to get a preliminary idea of what metal could be. The second type of information allowed this initial mathematical assessment of the plots to be refined. It consisted of clicking on the *Graphs* button, visually comparing the appearance of the plots of the Test material (solid lines) with those of each of the materials in the database (dotted lines, Fig. 8). Similar materials should not have plots crossing each other, except at the beginning. On the contrary, the graphs should be parallel, particularly at the end. The two types of information should be examined one after the other, as the proposals in the list provided can be discarded when studying the plots.

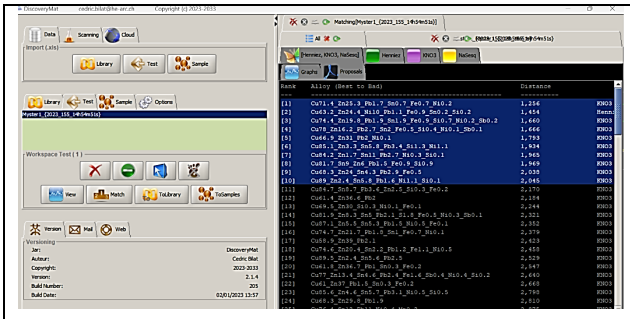

Fig. 7: List of proposed compositions of the metal under investigation given by the Discovery Mat application.

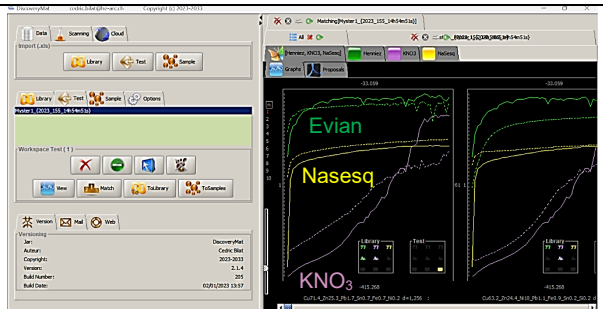


Fig. 8: Visual comparison of the plots of the metal under investigation with the materials in the database.

Among the 10 first proposals, the trend is for a quaternary alloy containing both Zn, Sn and Pb in different proportions. The distance between the plots of the studied metal and those of the materials of the database is above 1400 which does not correspond to a good matching (should be below 500). When examining the graphs, it appears that between proposal1 with Zn25.3 and Pb1.7 and proposal6 with Zn30, there is a better matching with the latter, particularly with KNO3. Another option would be proposal13 with Zn39 and Pb2.1 but the plots in Evian water give different trends.

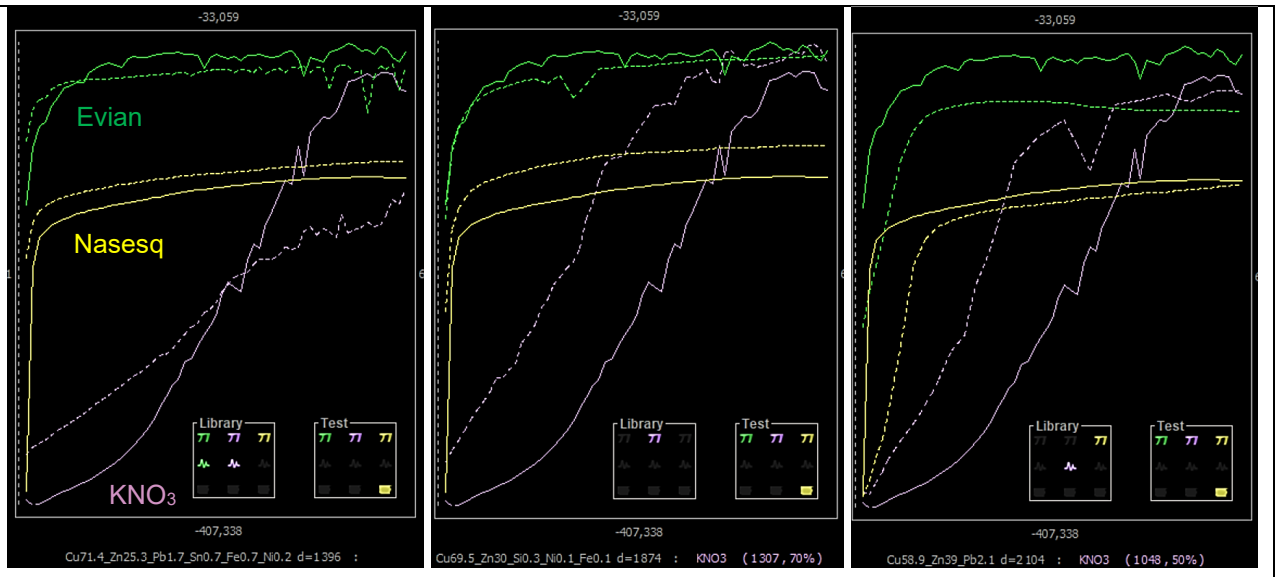


Fig. 9: Comparison of the plots of the studied metals with proposals 1, 6 and 13 from the Discovery Mat database.

X-ray fluorescence (XRF) analysis using a Thermo Niton XL3t GOLDD+ portable XRF instrument identified the composition of the sample as: Cu58 Zn38 Pb2.5 Sn0.5 Fe0.5 Ni0.4.

It appears then that proposals 6 and 13 are indeed rather relevant. The lack of an exact match with the database is probably due to the fact that many of the materials stored in the database were studied before Discovery Mat was developed, i.e. the electrochemical measurements were taken manually rather than automatically. The missing points (among the 900) were added later, sometimes without taking into account the rapid fluctuations in potential (such as in Evian water).

**2) 2nd of June:**

**- Pleco instrument to identify corrosion products formed on a tarnished silver coupon, and then to electrolytically reduce them in order to clean the silver surface**

The work began with measuring the potential a glassy carbon (GC) electrode against a Metrohm Ag/AgCl reference electrode by open circuit measurement (OCP) (Fig. 10). After calculating the value of the potential of GC electrode (448mV vs NHE), it was used as the reference electrode in the Pleco instrument. This was followed by characterizing the tarnishing on a silver metal coupon by linear sweep voltammetry (LSV). Then the tarnishing reduction process was monitored by chronoamperometry at the potential characteristic of the silver tarnishing ($Ag_2S$) present on the coupon, i.e. at the middle of its reduction peak measured by the LSV. The chronoamperometry measurement allowed to evaluate the cleaning level of the tarnishing, therefore stopping the reduction process at a low stable current value indicating the completion of the reduction process. Fig. 11 shows the setup for the characterisation and cleaning of the tarnished silver sample using the Pleco instrument.

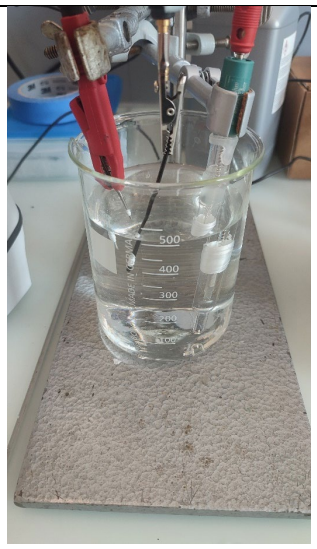

Fig. 10: Measuring the value of the potential for the GC electrode

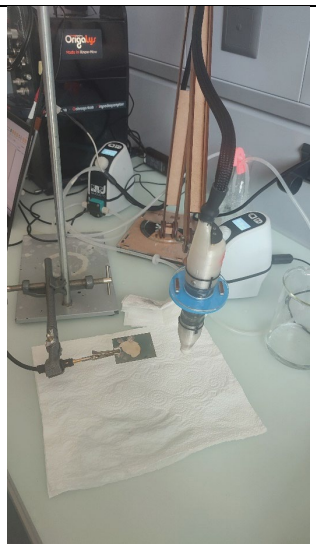

Fig. 11: The setup for tarnish removal using the Pleco instrument

**- Using the MiCorr application to identify the family of the metals studied by the Visual Inspection searching tool**

The tool was used to identify heritage metals objects based on their visual observation and physical characteristics, with the aid of investigating tools such as a magnet, a flashlight and a magnifier. By answering the questions of the search questionnaire, we were able to identify the families of three heritage metal artefacts: a corroded tinned iron sheet representing a putti blowing in a trumpet, an aluminium spices box and a silver 800 pie server with surface enrichment. Figs. 12-14 show the studied artefacts.

Fig. 12: Tinned iron artefact.


Fig. 13: Aluminium can.

Fig. 14: Silver pie server.

**3) 5th to the 9th of June:**

**Detailed work on the MiCorr application to create stratigraphic representations of the corrosion structures of two archaeological brass artefacts from Jordan in order to diagnose them**

This was the main part of the STSM, which aimed to create stratigraphic representations of the corrosion structures of two brass artefacts from Jordan, a buckle and a button (Figs. 15-16). They are part of a metal artefacts collection excavated from the Khirbet Yajuz archaeological site, which is located 11 km northwest of Amman, Jordan. They were excavated in 1996 from the Byzantine cemetery at site. Since then, they have been placed in the storage area of the University of Jordan Archaeological Museum (UJAM) in Amman.


Fig. 15: The studied buckle.


Fig. 16: The studied button.

The work included the following steps:

1) Determining the study areas of each artefact

On the surface of each artefact, three spots were analyzed using XRF and a cross-section sample was taken, embedded in an epoxy resin, then after curing, polished and prepared for analytical investigation and cross-section stratigraphy representation. Fig. 17-18 show the study areas of each artefact.

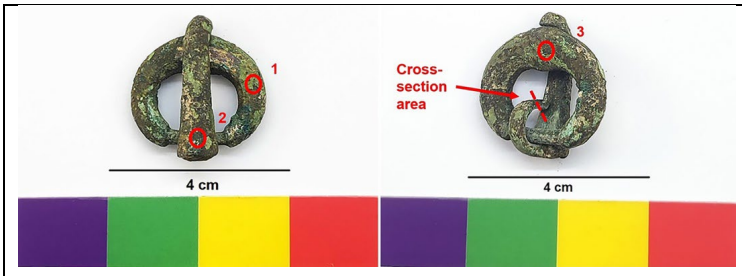


Fig. 17: Study areas of the buckle.

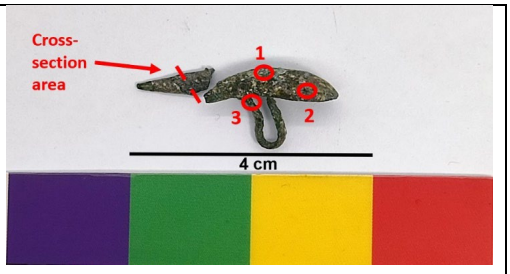


Fig. 18: Study areas of the button.

2) Observation of the artefacts and their corrosion forms with the aid of a binocular microscope to create a conceptual representation of their corrosion stratigraphy

Tables 1-2 and the schematic representations in Figs. 19-22 below, describe the corrosion structures encountered on the artefacts from the first visual macroscopic observation.

Table 1: Description of the principal characteristics of the buckle's strata
as observed under binocular and described according to Bertholon's method (Bertholon 2000).

| Strata | Type of strata | Principle characteristics |
|---|---|---|
| **S1** | Soil | Light brown soil sediments intermixed with CP1 |
| **CP1** | Corrosion product | White corrosion spots |
| **CP2** | Corrosion product | Olive-green corrosion layer |
| **CP3** | Corrosion product | Black corrosion layer |
| **CP4** | Corrosion product | Blue-green corrosion product |
| **CP5** | Corrosion product | Blue corrosion product |
| **CP6** | Corrosion product | Red-brown corrosion product |
| **M1** | Metal | Yellow metal |

Table 2: Description of the principal characteristics of the button's strata
as observed under binocular and described according to Bertholon's method (Bertholon 2000).

| Strata | Type of strata | Principle characteristics |
|---|---|---|
| **S1** | Soil | Light brown soil |
| **CP1** | Corrosion product | White corrosion spots |
| **CP2** | Corrosion product | Olive-green corrosion layer |
| **CP3** | Corrosion product | Blue-green corrosion product |
| **CP4** | Corrosion product | Red-brown corrosion product |
| **M1** | Metal | Yellow metal |

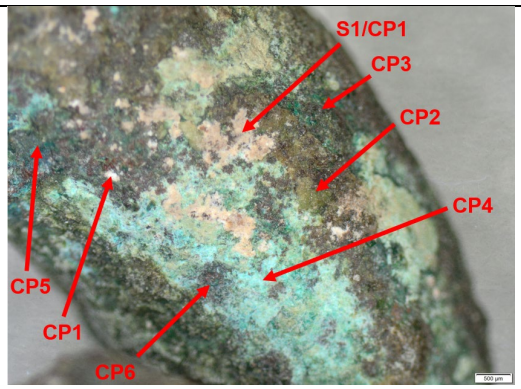


Fig. 19: Location of the different strata of the buckle listed in Table 1 and schematically represented on figure 21.

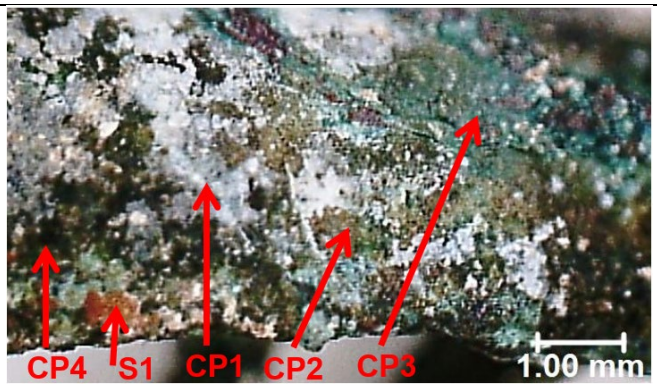


Fig. 20: Location of the different strata of the button listed in Table 2 and schematically represented on figure 22.

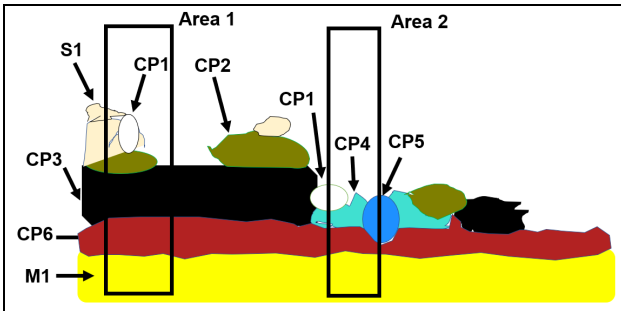


Fig. 21: Stratigraphic representation of the corrosion structure of the buckle based on visual observation with indication of areas 1 and 2 depicted using the MiCorr application in Fig. 23.

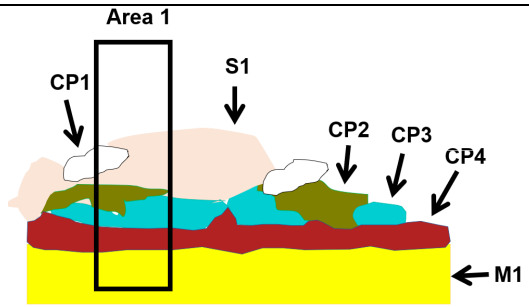


Fig. 22: Stratigraphic representation of the corrosion structure of the button based on visual observation with indication of area1 depicted using the MiCorr application in Fig. 24.

3) Based on the binocular observation of the strata on the artefacts, a digital representation of the corrosion stratigraphy from the MiCorr modelling programme was created

Two areas were selected on the buckle to represent the stratigraphy at different parts of the surface (Fig. 23), while one area was sufficient to represent the complete stratigraphy on the surface of the button (Fig. 24).

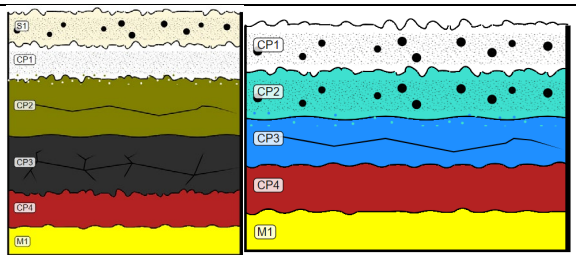


Area 1 Area 2

Fig. 23: Stratigraphic representation of the corrosion structure of the buckle observed macroscopically under binocular microscope using the MiCorr application. These representations can be compared to Fig. 21 considering that CP4 for Area 1 in Fig. 23 is CP6 in Fig. 21 and CP2, CP3 and CP4 for Area 2 in Fig. 23 are CP4, CP5 and CP6 respectively in Fig. 21.

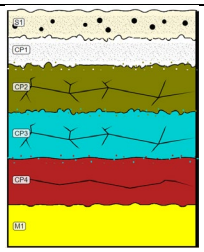


Area 1

Fig. 24: Stratigraphic representation of the corrosion structure of the button observed macroscopically under binocular microscope using the MiCorr application. This representation can be compared to Fig. 22.

## 4) Analysis and results

The two artifacts and their prepared and polished cross-section samples were analysed using several analytical techniques. The analyses performed were:

*- Non-Invasive methods*

XRF: with handheld portable X-ray fluorescence spectrometer (NITON XL3t 950 Air GOLDD+, Thermo Fischer®). General Metal mode, acquisition time 60s (filters: Li20/Lo20/M20). XRF analysis was carried out on the surface of the buckle and button (Figs. 17-18). All strata (deposit, corrosion products and metal) were analysed at the same time. From the results, the buckle is presumably a quaternary Cu-Zn-Sn-Pb alloy (Table 3), while the button should be a brass (Cu-Zn) alloy as the concentration of Pb and Sn is much less (Table 4). Other elements are from the environment.

Table 3: Chemical composition of the surface of the buckle analysed with XRF at three representative points shown in Fig. 17.

| Element | buckle 1 | buckle 2 | buckle 3 |
|---|---|---|---|
| **Cu** | 69 | 70 | 69 |
| **Zn** | 8 | 6 | 8 |
| **Pb** | 6.7 | 7.7 | 8.7 |
| **Sn** | 2.3 | 2.4 | 2.7 |
| **Si** | 11 | 13 | 7.6 |
| **P** | 0.7 | 0.5 | 2.3 |
| **Fe** | 0.2 | 0.3 | 0.3 |
| **Al** | 1.3 | 0 | 1.4 |

Table 4: Chemical composition of the surface of the button analysed with XRF at three representative points shown in Fig. 18.

| Element | Button a.1 | Button a.2 | Button a.3 |
|---|---|---|---|
| **Cu** | 65 | 70 | 64 |
| **Zn** | 15 | 14 | 19 |
| **Pb** | 1 | 1.2 | 0.6 |
| **Sn** | 0.2 | 1.7 | 0.5 |
| **Si** | 11 | 7 | 10 |
| **P** | 1.7 | 2 | 1 |
| **Fe** | 0.3 | 0.3 | 0.3 |
| **S** | 1.5 | 0.4 | 0.7 |
| **W** | 2 | 1.7 | 3.5 |
| **Al** | 2.3 | | |

*- Invasive methods*

- Optical microscopy (OM): the polished cross-sections were observed by OM in bright and dark field modes using a Leica DM/LP polarizing light microscope. The OM in dark field mode allowed to observe and quantify morphological, textural, microstructural and interfacial features of the strata in each cross-section. The cross-sections were then etched with ammonium persulphate 10% in water to examine their microstructures using bright-field illumination, which helped to identify the manufacturing techniques of the artefacts. Fig. 25 shows the STSM grantee investigating one of the samples with the scientific support from Prof. Christian Degrigny (HE-Arc CR) and the technical support from Mrs. Catherine Cséfalvay (Haute Ecole Ingénierie Arc).

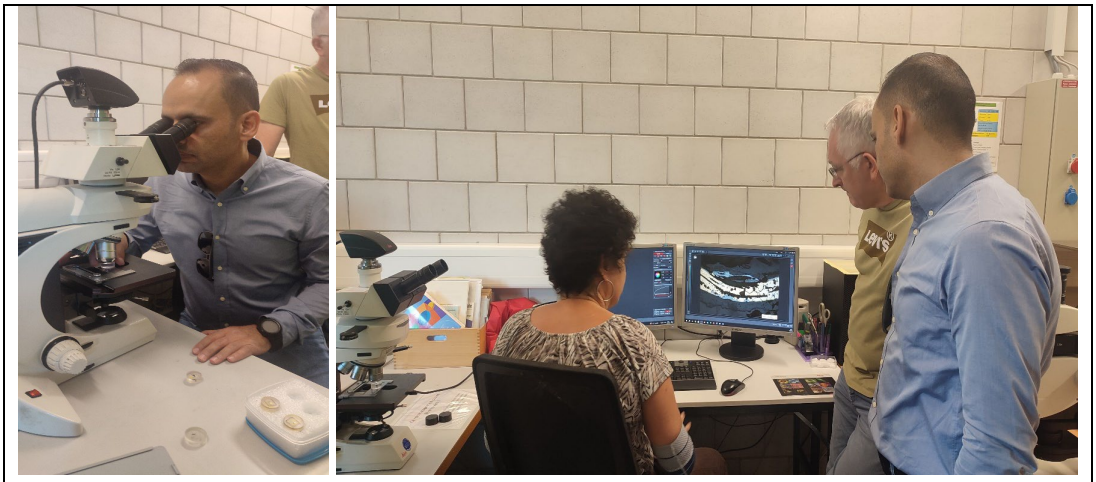

Fig. 25: Optical microscopy investigation of the cross-section of the button.

- SEM-EDS: the cross-section samples were coated with a Pt layer and the analysis of the internal alloy and corrosion layers was performed using a SEM-FEG JEOL 7001-F equipped with a silicon-drift EDS Oxford detector (Aztec analysis software) with an accelerating voltage of 20 kV and probe current at about 9 nA. The relative error is considered of about 10% for content range <1wt%, and 2% for content range of >1wt%. The SEM-EDS analysis allowed to observe chemical contrasts and determine elemental composition (main, secondary and additional elements) for the strata of the cross-sections. Fig. 26 shows the STSM grantee investigating one of the samples with the scientific support from Prof. Christian Degrigny (HE-Arc CR) and the technical support from Mrs. Catherine Cséfalvay (Haute Ecole Ingénierie Arc).

Fig. 26: SEM-EDS investigation of the cross-section of the buckle.

→ For the metal:

SEM-EDS analysis result of the internal alloy of the buckle showed that it consists of a quaternary Cu-Zn-Sn-Pb alloy (Table 5). Comparing the result with XRF surface analysis of the artefact shows a good agreement and indicates that there is no enrichment of Sn on the surface of the metal, which is usual for bronze artefacts. Furthermore, the core of the metal seems rather homogeneous. Fig. 27 indicates the area chosen for metallographic studies.

Table 5: EDS analysis result of the internal alloy of the buckle.

| Element | Wt. % |
|---|---|
| Cu | 83 |
| Zn | 9 |
| Pb | 5 |
| Sn | 3 |

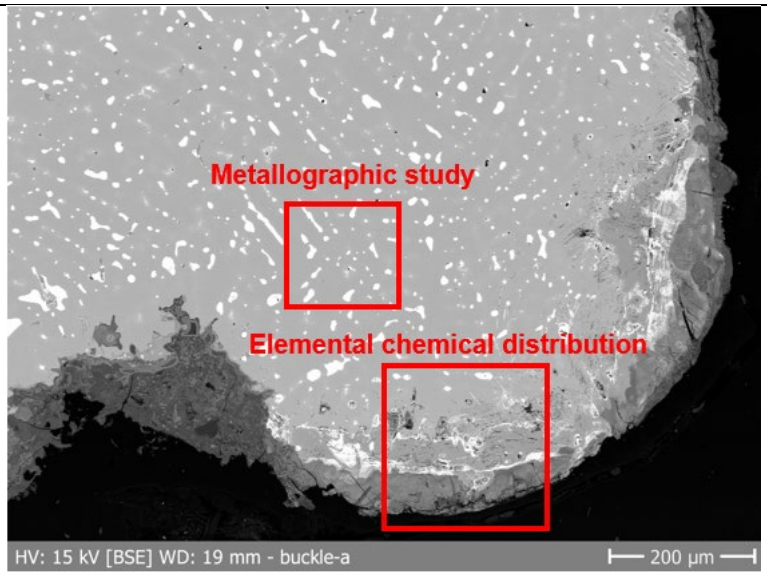


Fig. 27: SEM image of the cross-section of the buckle showing the areas for metallographic study (Fig. 29) and elemental chemical distribution (Fig. 32)

SEM-EDS analysis result of the internal alloy of the button showed that it consists of a brass (Cu-Zn) alloy (Table 6). The result of the SEM-EDS analysis is in a good agreement with the non-invasive XRF analysis result. The core of the metal is rather corroded. Fig. 28 indicates the area chosen for metallographic studies.

Table 6: EDS analysis result of the internal alloy of the button.

| Element | Wt. % |
|---|---|
| Cu | 77.5 |
| Zn | 22.5 |

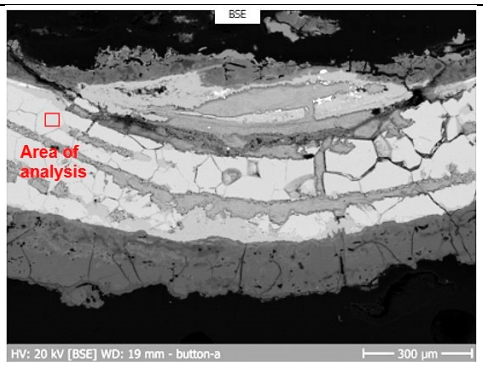


Fig. 28: SEM image of the cross-section of the button showing the area for metallography study (Fig. 30).

The OM examination results of the etched cross-section of the two artefacts showed an as-cast dendritic microstructure for the buckle, with the presence of air porosity and grey lead globules (Fig. 29). The presence of cored dendrites and strain lines suggests that the artefact was cold-worked without annealing. The button was annealed as indicated by its recrystallized microstructure and annealing twins (Fig. 30). The presence of intergranular cracks is attributed to the selective corrosion process, i.e dezincification (Scott 1991: 7–8; Scott & Schwab 2019: 154).

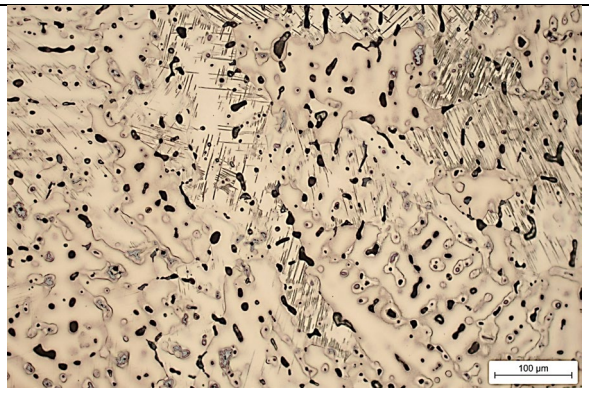


Fig. 29: OM image of the etched cross-section of the buckle.

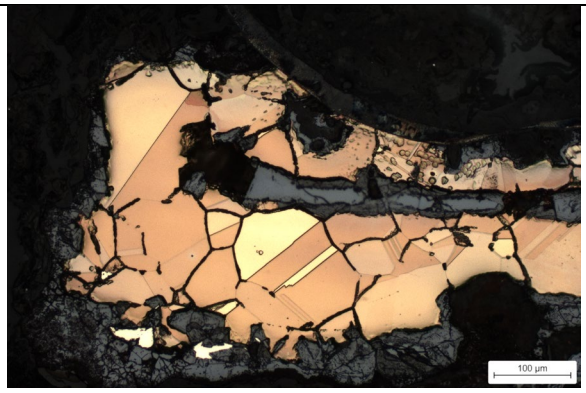


Fig. 30: OM image of the etched cross-section of the button.

→ For the corrosion layers:

The optical microscopy and SEM-EDS elemental mapping examination results of the buckle showed the presence of the phenomenon of dezincification, i.e. a selective leaching of the more active metal, zinc, from the alloy in the CP3 together with a decuprification phenomenon. CP1 layer showed the presence of Cu, Zn, Pb, C, O, P, and Cl, which could be attributed to the presence of corrosion products of copper, zinc, and lead (carbonates, chlorides and phosphates). The Si, Al, and Ca in S1 and CP1 are the elements of soil deposits on the surface of the artefact, i.e. aluminosilicate and calcite deposits. The red CP2 layer showed mainly the presence of Cu and O, which could indicate a cuprous oxide corrosion layer (Figs. 31-32). It should also be noted that the presence of P and Ca in the CP1 layer could also indicate the effect of phosphate species released by the hydrolysis of hydroxyapatite ($Ca_5(PO_4)_3OH$) from the skeletal materials in the neighbouring bodies buried in the cemetery where the buckle was excavated from, which induced the formation of copper minerals containing them. It seems that the formation of insoluble phosphate corrosion products on the surface of the artefact improved its stability and reduced the risk of activating the cuprous chlorides present in the internal pits and the dezincification in the uncontrolled environment of the storage area. The original surface has been preserved and corresponds to the interface between CP1 and CP2 for both artefacts. The high concentration of Pb at the outer edge of the artefact is probably attributed to its manufacturing technique; it was cast in a mould where it was allowed to slowly cool, and due to gravity segregation, Pb pooled down to the bottom of the mould and solidified in the external part of the alloy (Abu-Baker and Khalil 2022; Abu-Baker 2023a; Abu-Baker 2023b).

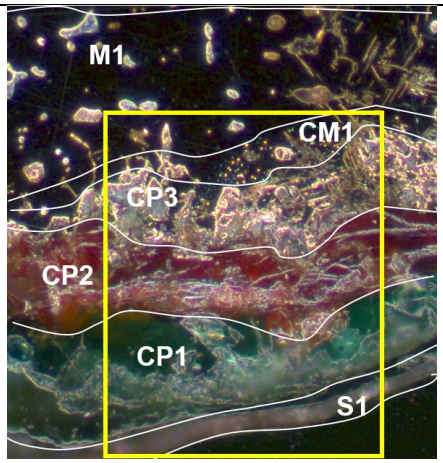


Fig. 31: Micrograph of the corrosion structure of the buckle's cross-section, unetched, dark field.

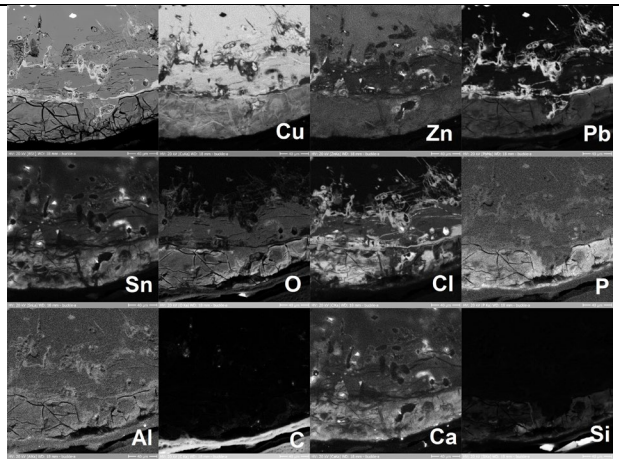


Fig. 32: SEM image, BSE-mode, and elemental chemical distribution of the selected area (Fig. 31) of the buckle's cross-section.

Similarly, the optical microscopy and SEM-EDS elemental mapping examination results of the button showed that CP1 corroded layer contained Cu, Zn, Pb, O, P, Si, Ca, and Al. The presence of P and Ca in the CP1 layer could be attributed to the hydrolysis of hydroxyapatite ($Ca_5(PO_4)_3OH$), which induced the formation of copper minerals containing them as mentioned for the buckle. The Ca could have also come from the calcite in the burial context of the archaeological site. The Si and Al in the S1 and CP1 are the elements of soil deposits as mentioned for the buckle. The CP2 is rich in Cu and O, which probably indicates the presence of cuprite ($Cu_2O$). The original surface has been preserved and corresponds to the interface between CP1 and CP2 for both artefacts. The CP3 is rich in Cu and Cl, while Zn is missing, which indicates an internal dealloying and selective removal of the more anodic metal (Zn), i.e., dezincification by the corrosion processes (Figs. 33-34). In the presence of chloride ions in the corrosion burial environment, the dissolution of the more anodic metal, zinc, from brass is higher than that of copper and the corrosion process is controlled by diffusion; i.e. $Zn^{+2}$ ion with an ionic radius of 0.070 nm is easier to diffuse than $Cu^{+1}$ ion that has a 0.096 nm ionic radius. The diffused zinc ions reacted with the corrosive burial soil and after a prolonged exposure, zinc corrosion products precipitated on the outer surface of the artefact or the surrounding soil. It seems that the formation of some insoluble phosphate corrosion products on the surface of the artefact improved its stability against the active chloride-based corrosion present in the internal pits, however its dezincification is more prominent than the buckle as it has a higher zinc content, therefore it is more prone to corrosion in the uncontrolled environment of the storage area. (Abu-Baker et al. 2021; Abu-Baker and Khalil 2022).

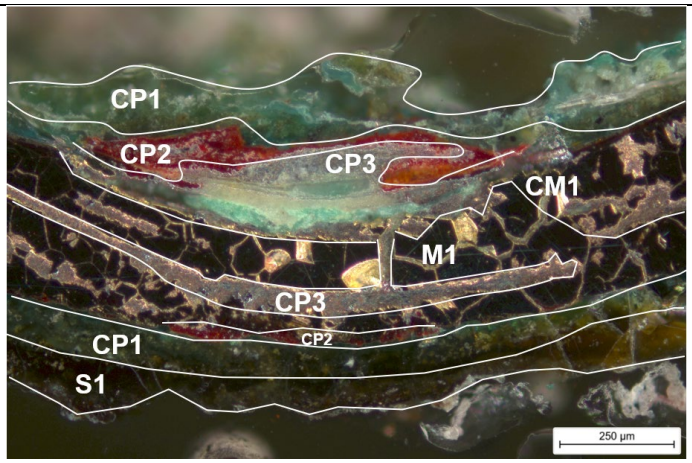


Fig. 33: Micrograph of the corrosion structure of the button's cross-section, unetched, dark field.

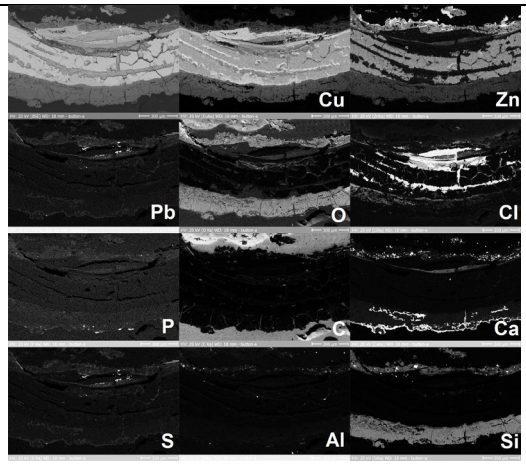


Fig. 34: SEM image, BSE-mode, and elemental chemical distribution of the selected area of the button's cross-section (Fig. 33).

5) Based on the microscopic examination of the strata on the cross-sections of the artefacts, digital representations of the corrosion stratigraphy from the MiCorr modelling programme were created

Fig. 35 shows the STSM grantee working on generating the digital representations of the corrosion stratigraphy from the MiCorr modelling programme and the produced stratigraphic representations for the cross-sections of the two artefacts (Figs. 36-37).

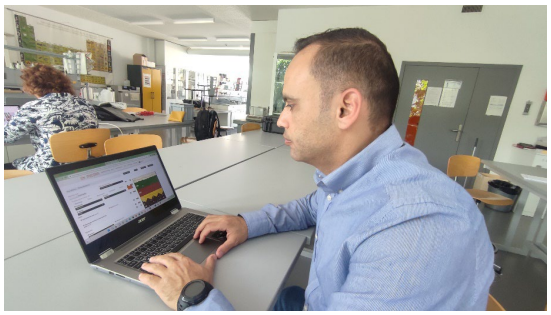

Fig. 35: Using the MiCorr application to create a digital representation of the corrosion stratigraphy.

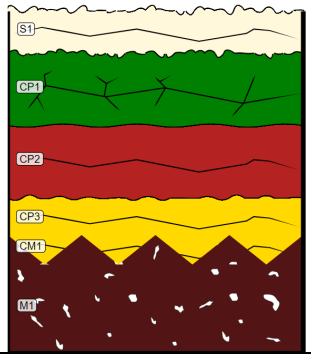


Fig. 36: Stratigraphic representation of the sample from the buckle in cross-section (dark field) using the MiCorr application. This representation was built according to Fig. 31.

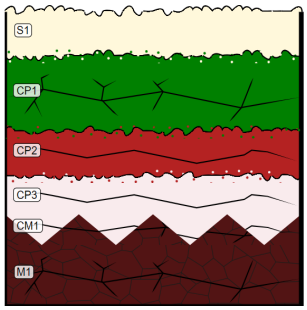


Fig. 37: Stratigraphic representation of the sample from the button in cross-section (dark field) using the MiCorr application. This representation was built according to Fig. 33.

6) Synthesis of the binocular/ cross-section examination of the corrosion structure for the two artefacts

→ For the buckle: The observation under binocular microscope identified 4 CPs of different colors (Area 1). Changing the position of binocular observation affected the color of the 4 CPs observed (Area 2). The cross-section identified 3 CPs. With binocular microscope, it is possible to differentiate strata according to texture and light color changes that do not always correspond to significant changes in chemical composition, thus leading to a regrouping of several strata into one in the cross-section observation and physicochemical characterization (Fig. 38). The differences between the two observation modes could also be explained by different locations of observation.

Both observation modes identified one S1 stratum. The S1 and CP1 of Area 1 or CP1 of Area 2 under binocular microscope correspond to S1 of the cross-section. The CP2 of Area 1 and CP2 and CP3 of Area 2 under binocular microscope probably correspond to CP1 of the cross-section. Similarly, the CP3 and CP4 of Area 1 or CP4 of Area 2 under binocular microscope probably correspond to CP2 of the cross-section. The CP3 of the cross-section was not observed under the binocular microscope and could not be linked as its characteristics are different.

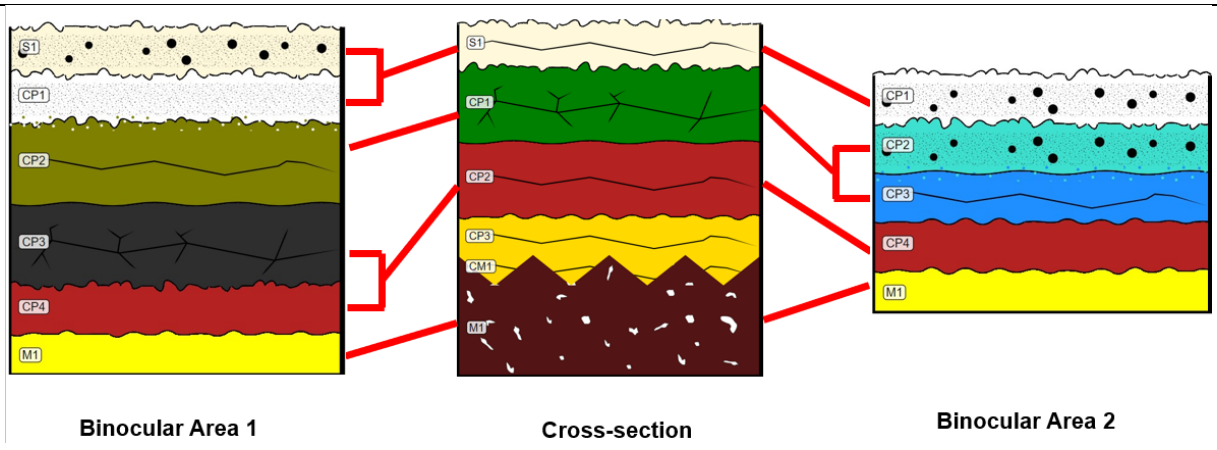


Fig. 38: Stratigraphic representation side by side of binocular views and cross-section (dark field) of the buckle.

→ For the button: The observation under binocular microscope identified 3 CPs of different colors, and the cross-section observation using the dark-field illumination of the optical microscope identified 3 CPs. Similar to the buckle's investigation, with binocular microscope, it is possible to differentiate strata according to texture and light color changes that do not always correspond to significant changes in chemical composition, thus leading to a regrouping of several strata into one in the cross-section observation and physicochemical characterization (Fig. 39). The differences between the two observation modes could also be explained by different locations of observation.

The S1 and CP1 under binocular microscope correspond to S1 of the cross-section. The CP2 and CP3 under binocular microscope could be grouped and probably correspond to CP1 in cross-section. Similarly, the CP4 under binocular microscope probably corresponds to CP2 and some parts of CP3 in cross-section.

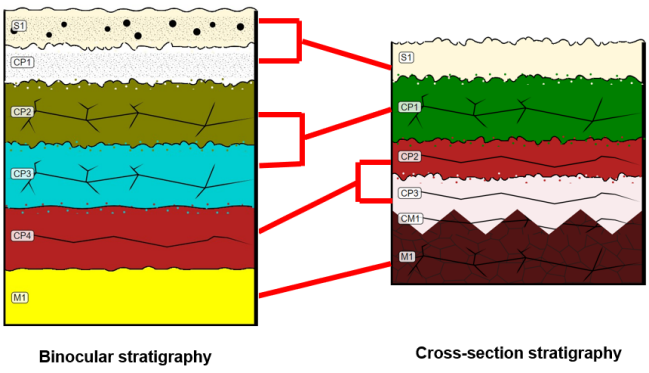


Fig. 39: Stratigraphic representation side by side of binocular view and cross-section (dark field) of the button

Conclusion

The buckle is a quaternary alloy of Cu-Zn-Sn-Pb with Zn as the highest alloying element (8-9 wt%), while the button is made of a brass alloy (Cu-Zn) with high zinc content (22.5%). After observing the corrosion structure in cross-section, it is possible to identify the original surface that has been preserved and corresponds to the interface between CP1 and CP2 for both artefacts. As for the corrosion structure underneath, it presents the phenomenon of dezincification commonly observed in brasses, i.e. a selective leaching of the more active metal, zinc, from the alloy. The elemental distribution of Cu and Zn in the X-ray maps showed patterns of depletion across the alloy, which is more prominent in the button as it has a higher zinc content, therefore is more prone to the dezincification phenomenon. The formation of the insoluble phosphate corrosion products on the surface of the artefacts increased their stability and reduced the risk of activating the cuprous chlorides present under the external corrosion layers and the dezincification of these artefacts in the environmentally uncontrolled storage area. The investigation of the internal corrosion was complementary to that of external corrosion and helped in providing complete information about the corrosion of these artefacts. These corrosion stratigraphy representations and accompanying information will form two new files which will be added to the MiCorr database and made available to other users.

**Description of the STSM main achievements and planned follow-up activities**

The STSM allowed the grantee to use the three ENDLESS Metal analytical tools under professional supervision. It also offered access to the Haute Ecole Arc Conservation-Restauration laboratories where the training and use of the tools took place. The knowledge obtained on MiCorr application was applied on two archaeological artefacts from Jordan. It will be applied on more artefacts in the future and the information on the tool will be passed to other professional colleagues and students. The STSM will open venues for networking and fostering research collaboration between Yarmouk University and Haute Ecole Arc in the future.

**References**


Abu-Baker, A. N. 2023a, A technical examination of the corrosion and microstructural features of copper alloy artifacts from the Byzantine period at Khirbet Yajuz, Jordan, *Metallography, Microstructure, and Analysis*. vol.12, pp. 276–288.

Abu-Baker, A. N. 2023b, Analytical investigation and electrochemical conservation treatment for archaeological copper alloy artifacts from Jordan, *Conservar Património,* vol. 42, pp. 38–55.

Abu-Baker, A. N. 2022, The corrosion characteristics and electrochemical conservation treatment for an archaeological lead ossuary from Jordan, *Ge-conservación***,** vol. 22, no. 1, pp. 154–161.

Abu-Baker, A. N. and Khalil, L. A. 2022, An analytical study of the corrosion behavior and microstructural properties of a group of copper alloy artifacts from the Khirbet Yajuz archaeological site, Jordan, in *Metal2022: Proceedings of the Interim Meeting of the ICOM-CC Metals Working Group, 5–9 September 2022*, ed. by P. Mardikian, L. Näsänen, and A. Arponen, (International Council of Museums – Committee for Conservation (ICOM–CC) and The National Museum of Finland, Helsinki, pp. 221–230.

Abu-Baker, A. N., Khalil, L. A. and Gonmeen, T. 2021, A multi-analytical exploration of the chemical composition, microstructural properties and corrosion inhibiting treatment for an archaeological brass censer from Umm Zuwaytinah, Amman, *Nuclear Inst. and Methods in Physics Research, B*, vol. 502, pp. 73–79.

Bertholon, R. 2000, La limite de la surface d'origine des objets métalliques archéologiques, caractérisation, localisation et approche des mécanismes de conservation. PhD dissertation, University Paris 1 Panthéon-Sorbonne, France. https://theses.hal.science/tel-00331190v1/document (accessed 01/06/2023).

Scott, D. A. 1991, *Metallography and microstructure of ancient and historic metals*, The Getty Conservation Institute, Los Angeles.

Scott, D. A.; Schwab, R. 2019, *Metallography in art and archaeology (cultural heritage science)*, Springer Nature, Switzerland.